J Physiol 586.22 (2008) pp 5367–5381

The Journal of Physiology

Kinetics of Rab27a-dependent actions on vesicle docking and priming in pancreatic β-cells

Matthew J. Merrins and Edward L. Stuenkel

Department of Molecular and Integrative Physiology, University of Michigan, Ann Arbor, MI 48109, USA

The small GTPase Rab27a, along with the isoforms of Rab3, is present on insulin secretory granules and has been implicated in regulation of Ca^{2+}-triggered exocytosis. We have used membrane capacitance measurements to define the role of Rab27a in regulating the size and refilling of distinct pools of insulin granules by comparison of evoked secretory responses from Rab27a-null *ashen* and strain-matched wild-type control pancreatic β-cells. We find that *ashen* β-cells display a kinetic defect in refilling of readily releasable and immediately releasable vesicle pools (RRP and IRP, respectively) in response to depolarization-evoked Ca^{2+} influx. The deficit in IRP refilling was not observed in the presence of stimulatory glucose concentrations (16.7 mM), though incomplete refilling of the RRP persisted. Comparatively, β-cells from Rab3a$^{-/-}$ mice exhibited complete refilling of the IRP and RRP, demonstrating that Rab27a and Rab3a exert distinct roles in the insulin granule secretory pathway. Further, depletion of the RRP in *ashen* β-cells was twofold faster than that of control β-cells. These deficits in refilling and exocytotic rate in *ashen* β-cells were absent when cAMP-regulatory pathways were activated. Elevated cAMP increased the RRP pool size, and complete refilling of the RRP occurred in *ashen* β-cells; responses were comparable to wild-type controls. These effects of cAMP were largely eliminated by Rp-cAMP inhibition of PKA, indicating that PKA acts on vesicle priming downstream or via pathways independent of Rab27a. In summary, Rab27a exerts dual roles in glucose-mediated insulin granule exocytosis, facilitating refilling of releasable granule pools while also limiting the rate of release from these pools.

(Received 20 June 2008; accepted after revision 18 September 2008; first published online 18 September 2008)
Corresponding author E. L. Stuenkel: Department of Molecular and Integrative Physiology, 7744 MSII, 1153 W. Medical Center Drive, Ann Arbor, MI 48109–0622, USA. Email: esterm@umich.edu

Glucose initially evokes insulin release from pancreatic β-cells by increasing ATP production, which closes K_{ATP} channels and results in the opening of voltage-dependent Ca^{2+} channels, stimulating Ca^{2+}-triggered insulin granule exocytosis. Kinetically slower secretion-amplifying pathways that are dependent on glucose metabolism but independent of the K_{ATP} channel also occur, and their relevance has been extensively reviewed (Eliasson *et al.* 1997; Takahashi *et al.* 1997). Additionally, hormones and neurotransmitters modulate the magnitude of secretion through a number of G-protein coupled receptor pathways (Ammala *et al.* 1993*a*; Renstrom *et al.* 1997; Wan *et al.* 2004; Yang & Gillis, 2004; Shibasaki *et al.* 2007). The secretory response of the β-cell results from the release of insulin from secretory granules occupying distinct, functionally defined granule pools. These pools include release competent granules in the 'readily releasable' pool (RRP), a subset of which comprise the 'immediately releasable' pool (IRP) that is spatially positioned adjacent to Ca^{2+}-channels. A third pool distinct from the RRP has been identified and termed the highly Ca^{2+}-sensitive pool (HCSP) (Wan *et al.* 2004; Yang & Gillis, 2004). The number of secretory granules in each pool, the rate of pool refilling, and the rate at which fusion is regulated from these pools largely determines the secretory response of a β-cell.

Rab proteins, which belong to the Ras-related superfamily of small monomeric GTPases, are central mediators of membrane trafficking in all eukaryotic cells. Rab proteins continuously cycle between GTP and GDP bound states, interacting and activating effector molecules when GTP-bound (Fukuda, 2005). With respect to regulated exocytosis, Rab proteins regulate a series of steps including: vesicle/granule transport along cytoskeletal tracts, physical attachment of the vesicles/granules to the plasma membrane (i.e. docking/tethering), priming reactions that allow assembly of the molecular machinery for membrane fusion, and soluble *N*-ethylmaleimide-sensitive factor attachment protein receptor (SNARE)-catalysed fusion (Burgoyne & Morgan, 2003). Rab27a and four isoforms of Rab3 (a/b/c/d) are localized to secretory granules in a number of cell types, and have been directly implicated

DOI: 10.1113/jphysiol.2008.158477

in the regulation of Ca^{2+}-dependent exocytosis in β-cells (Fukuda, 2005). While Rab27a mutants locked in the GTP-bound and GDP-bound states strongly facilitate and potently inhibit insulin secretion, respectively (Yi *et al.* 2002; Fukuda, 2003), it is becoming increasingly apparent that it is the rate at which GTP/GDP cycles on Rab proteins that determines the level of their control on physiological function (Kondo *et al.* 2006).

Rab27a deficiency results in multiple defects in *ashen* mice (Wilson *et al.* 2000), which are glucose intolerant owing to strongly reduced first- and second-phase glucose-stimulated insulin secretion (Kasai *et al.* 2005). Part of the β-cell secretory defect is reportedly due to a deficit in the replenishment of docked granules, a phenotype evident in other Rab27a-null secretory cells including melanosomes and cytotoxic T-lymphocytes (resulting in the ashen coat-colour and immunodeficiency) (Hume *et al.* 2001; Stinchcombe *et al.* 2001; Wu *et al.* 2002). In addition, there are indications that insulin granule priming may be reduced in *ashen* β-cells based on total internal reflection microscopy (TIRFM) imaging showing a reduced release of insulin granules that are docked to the plasma membrane in *ashen* β-cells with respect to control β-cells (Kasai *et al.* 2005). Consistently, ablation of certain Rab or Rab effectors (e.g. Munc18, syntaxin, Munc13) reduces vesicle docking and priming (Voets *et al.* 2001; de Wit *et al.* 2006; Kang *et al.* 2006; Gulyas-Kovacs *et al.* 2007).

To evaluate the dynamic effects of Rab27a on secretion we have used high temporal resolution membrane capacitance measurements to measure secretion from single pancreatic β-cells isolated from *ashen* mice. This approach has allowed us to precisely define the role of Rab27a in regulating the size, rate of release from and refilling of insulin granule pools. Our results are novel in demonstrating (1) that *ashen* β-cells exhibit a time-dependent kinetic defect in vesicle priming into both the IRP and RRP granule pools, and (2) that Rab27a regulates the rate of insulin granule release from the RRP.

Methods

Mice and tissue preparation

All experiments were carried out according to rules and regulations of the University Committee on Use and Care of Animals (UCUCA). The *ash/ash* mice (C3H/He background) were kindly provided by N. A. Jenkins (National Cancer Institute, Frederick, MD, USA) in cooperation with Jackson Laboratories (Bar Harbor, ME, USA). The mice were maintained on the C3H/He strain by forced heterozygosis (mating homozygous males to heterozygous females), and age matched C3H/He mice were used as background controls. In *ashen* mice (Wilson *et al.* 2000; Kasai *et al.* 2005), a single A-to-T transversion in the splice donor site downstream of exon 4 results in a larger than normal transcript due to the insertion of 235 or 252 base pairs of intron into the Rab27a message. An in-frame stop codon in the intron sequence leads to the production of a non-functional Rab27a protein lacking two critical domains of the GTP-binding pocket. $Rab3a^{-/-}$ mice (C57Bl/6 background) and control C57Bl/6 mice were provided by K. Engisch (Wright State University, Dayton, OH, USA) (Wang *et al.* 2008). Mice were killed by cervical dislocation and islets were isolated by retrograde perfusion of the pancreatic duct with 4 ml 0.6–8 mg ml^{-1} collagenase (Roche Liberase RI, Roche Diagnostics) in physiological saline solution (PSS; in mM: 137 NaCl, 5.6 KCl, 1.2 $MgCl_2$, 0.5 NaH_2PO_4, 4.2 $NaHCO_3$, 2.6 $CaCl_2$, 2.5 glucose, pH 7.4, 310 mosmol l^{-1}). The pancreas was immediately excised and further digested for 35–40 min at 37°C. Islets were hand-picked after washing the tissue twice in 20 ml PSS containing 5 mg ml^{-1} BSA. One hundred and thirty to one hundred and eighty islets were dispersed into single cells and small clusters by 10 min incubation at room temperature in 10 ml Ca^{2+}-free PSS (PSS lacking $CaCl_2$ and containing 2 mM EGTA), followed by 5 min gentle shaking in 1 ml Ca^{2+}-free PSS containing 0.025% trypsin at 37°C (Invitrogen). The dispersed cells were washed twice in 10 ml RPMI 1640 media containing 5 mM glucose and 10% (v/v) fetal bovine serum (FBS) supplemented with penicillin (100 U ml^{-1}) and streptomycin (100 μg ml^{-1}), before plating on glass-bottomed dishes coated with poly-L-lysine. Cells were kept in a 37°C incubator at 5% CO_2 and recorded from 2 to 3 days after preparation.

Imaging of intracellular Ca^{2+}

Mouse pancreatic β-cells plated on glass-bottomed dishes were incubated in PSS containing 2 μM Fura-2-AM (Molecular Probes) for 15 min at 37°C. Subsequently the dish volume was reduced to 0.5 ml, and the cells were equilibrated in PSS at a flow rate of 1 ml min^{-1} in a heated chamber (30–33°C). After >10 min, cells were incubated in PSS containing 16.7 mM glucose, and fluorescence of individual β-cells was elicited using alternating excitation wavelengths of 340 and 380 nm (Till Polychrome V, Till Photonics, Gräfelfing, Germany), a 410-dLcp beamsplitter, and a D510/80 wide band emission filter (Chroma Technology Corp., Rockingham, VT, USA). Emission intensity was collected with a Quant-EM camera (Photometrics, Tucson, AZ, USA) at 2 Hz.

Electrophysiology

Whole-cell patch clamp measurements were performed at 30–33°C using an EPC-9 amplifier and Patchmaster acquisition software (HEKA Elektronik, Lambrecht/Pfalz, Germany). Pipettes (3–5 MΩ) were pulled from

borosilicate glass (A-M systems, Carlsborg, WA, USA), coated with Slygard 184 (Dow Corning, Midland, MI, USA), and fire-polished. The pipette was held at a DC potential of −70 mV except during membrane depolarization. Capacitance measurements were performed using the software Lock-in extension of the Patchmaster software (dc + sine) using a sinusoid applied with an amplitude of 20 mV and a frequency of 1250 Hz. R_s was typically < 10 MΩ.

All reagents were from Sigma unless stated otherwise. The standard bath solution consisted of 113 mM NaCl, 5.5 mM KCl, 1.2 mM $MgCl_2$, 4.8 mM $NaHCO_3$, 10 mM $CaCl_2$, 20 mM TEA-Cl, 5 mM glucose, and 10 mM Hepes titrated to pH 7.3 with NaOH (310 mosmol l^{-1}). The standard pipette solution contained 125 mM caesium glutamate, 10 mM CsCl, 10 mM NaCl, 0.25 mM EGTA, 0.16 mM $CaCl_2$, 3 mM Mg-ATP, 0.01 mM Na-GTP, and 5 mM Hepes titrated to pH 7.2 using CsOH (300 mosmol l^{-1}). The initial $[Ca^{2+}]_i$ was estimated to be 272 nM (WebMAXC software). TEA^+ and Cs^+ eliminated the contribution of K^+ efflux, allowing calculation of Q_{Ca} by integration of leak-subtracted ($P/4$) I_{Ca} during a 15 ms depolarizing pulse given 1 min after membrane rupture and 2 min prior to the stimulus train. As previously described (Kinard & Satin, 1995; Miley *et al.* 1999), a large slow onset Cl^- influx was observed during the stimulus protocol (Fig. 1*A*), possibly activated by our intracellular clamp of ATP at 3 mM as well as the cell-swelling associated with the whole-cell patch configuration, prohibiting quantification of I_{Ca} during measurement of the RRP. In some experiments, the pipette solution was supplemented with 100 μM cAMP, 100 μM 8-pCPT-2′-*O*-Me-cAMP (Axxora), or 500 μM Rp-cAMP (Axxora, San Diego, CA, USA).

Statistics

Statistical analysis was performed using InStat (GraphPad Software Inc., San Diego, CA, USA). Student's two-tailed paired *t* test, assuming Gaussian distribution (parametric), was used to determine differences between mean IRP and RRP size measured from pairs of depolarization trains (see Fig. 1*A*) on each cell. A two-tailed unpaired *t* test, assuming equal standard deviations, was used to compare mean IRP and RRP size between treatments (e.g. wild-type *versus ashen*).

Results

Ashen mice display a time-dependent kinetic defect in vesicle pool refilling

Our initial goal was to determine the kinetic parameters within the exocytotic pathway that are specifically altered by Rab27a deficiency using cultured mouse β-cells isolated from control C3H/He and *ashen* mice, which lack functional Rab27a protein (Wilson *et al.* 2000). High-resolution membrane capacitance measurements were used to monitor exocytosis. We devised a voltage-clamp depolarization protocol to separately stimulate vesicle release from the immediately releasable and readily releasable pools (IRP and RRP, respectively), which consist of docked and primed granules. The stimulation protocol consisted of a series of five 50 ms depolarizations (ΔCm_5) to deplete the IRP, followed by eight 500 ms depolarizations (ΔCm_8) to elicit secretion from the RRP, each from a holding potential of −70 mV to +20 mV (Fig. 1*A*), with a 100 ms interpulse interval. In wild-type β-cells we observed a small capacitance increase (8 ± 1 fF, $n = 33$) after ΔCm_5 corresponding to release from the IRP (Fig. 1*B* and *D*). From Fig. 1*B* it can be seen that there is little additional capacitance change after the first two pulses, indicating depletion of the IRP without significant stimulation of release from the RRP. As an alternative estimation of the IRP size, a subset of the wild-type β-cell ΔCm_5 responses fit the criteria for a '2-pulse' protocol (using the first two successive 50 ms pulses which are separated by 100 ms) for estimating the IRP as previously described (Gillis *et al.* 1996). In a comparable fashion to measuring IRP at the end of ΔCm_5, this analysis estimated the IRP size (B_{max}) as 7 ± 1 fF ($n = 19$) in wild-type β-cells (Fig. 1*D*). The magnitude of the IRP in *ashen* β-cells was comparable to C3H/He cells as shown in Fig. 1*B* and *D*. Stimulated release from the RRP in wild-type cells (114 ± 24 fF, $n = 33$) was not significantly different from *ashen* cells (128 ± 22 fF, $n = 33$) using the ΔCm_8 stimulation train. The membrane conductance (G_m) in both control and *ashen* β-cells also exhibited similar patterns to the step depolarization protocol (Fig. 1*C*). Assuming 1.7 fF per granule measured previously in mouse β-cells (Ammala *et al.* 1993*b*), the fast kinetic phase corresponding to the IRP was estimated at ∼5 granules while ΔCm_8 released ∼75 granules, which by other reports of mouse β-cells employing flash photolysis corresponds to the majority and perhaps the entire RRP under the equivalent conditions of 5 mM glucose (Renstrom *et al.* 1997; Wan *et al.* 2004; Yang & Gillis, 2004). Interestingly, kinetic analysis of Fig. 1*B* indicates that secretion from *ashen* β-cells secretion progresses significantly faster (2×) than control C3H/He β-cells, based on single exponential fits of the ΔCm_8 secretory response (*ashen*, $1/\tau = 0.63 \pm 0.09\ s^{-1}$; C3H/He, $1/\tau = 0.32 \pm 0.06\ s^{-1}$). The increased rate of secretion in *ashen* β-cells indicates that Rab27a participates in a rate-limiting step in the final stages of glucose-regulated exocytosis.

Our above results are novel in indicating that the defect in glucose-stimulated insulin secretion previously observed in *ashen* islets (Kasai *et al.* 2005) is not due to

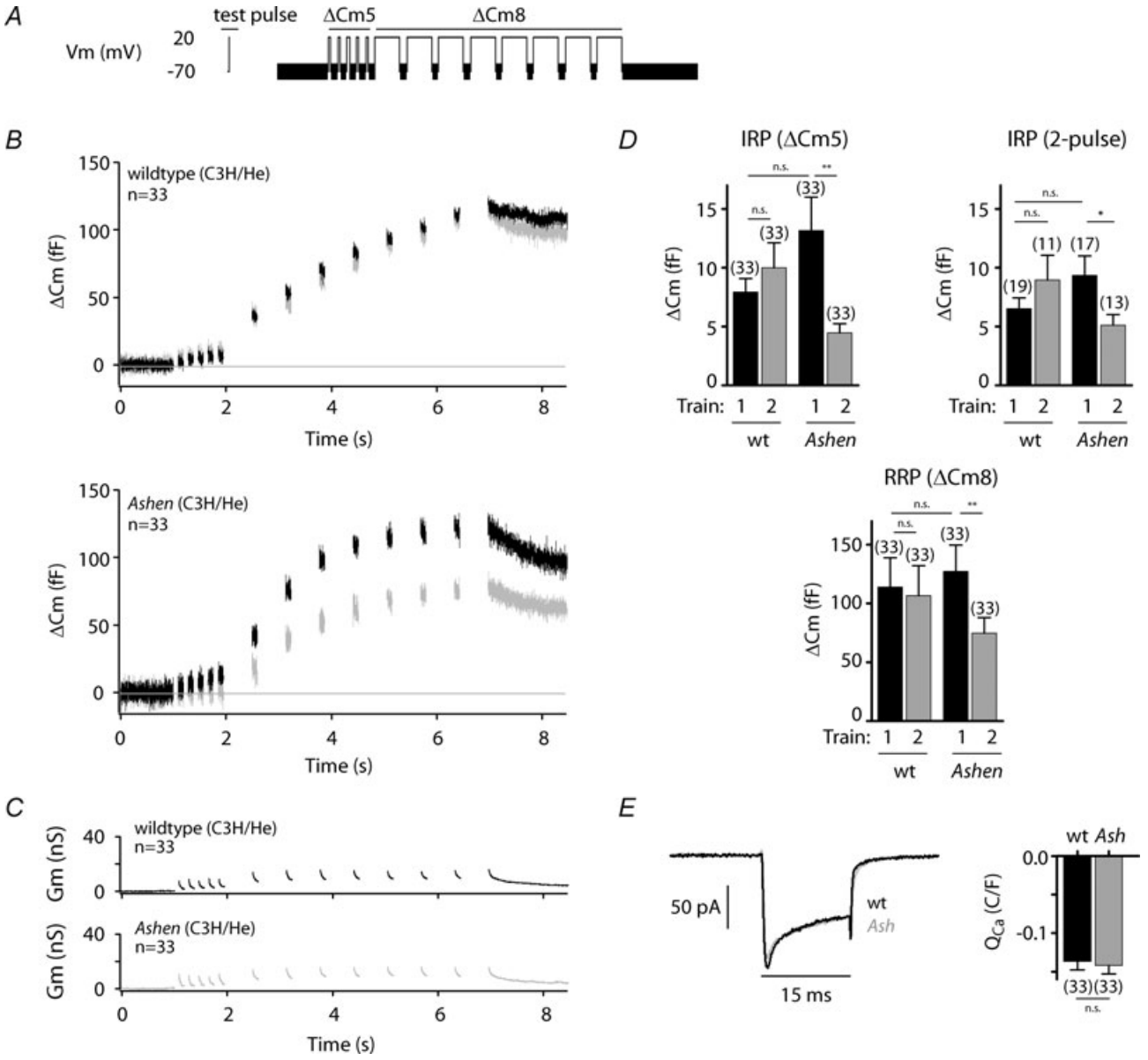

Figure 1. Ashen mice exhibit kinetic defects in refilling of the IRP and RRP
A, mouse pancreatic β-cells under whole-cell voltage clamp were depolarized from a holding potential of −70 mV to +20 mV to elicit exocytosis of β-granules. The stimulus train consisted of five 50 ms depolarizations (ΔCm_5) to exhaust the IRP, which was immediately followed by eight 500 ms depolarizations (ΔCm_8) to stimulate release from the RRP. The interpulse interval was 100 ms. The entire stimulus train was repeated twice for each experiment, allowing 2 min between trains for vesicle pool recovery. A 15 ms test depolarization was given 1 min after establishing whole-cell, and 2 min prior to the first stimulus train to measure the properties of I_{Ca}. *B*, averaged capacitance increases measured from wild-type (C3H/He) and *ashen* β-cells in response to the 2 pulse trains (black, grey) in *A*. *C*, averaged membrane conductance measured from wild-type (C3H/He) (black) and *ashen* (grey) β-cells during the first stimulus train in *B*. *D*, averaged capacitance increases measured after ΔCm_5 (IRP) or ΔCm_8 (RRP) from cells in *B*. The IRP was also estimated using the equation $S/(1 - R^2)$, where S is the sum of the first two capacitance responses and R is the ratio of the first two responses (2-pulse) (Gillis *et al.* 1996). Cells were selected for this analysis only when the capacitance increase following the first depolarizing pulse was greater than 60% of the capacitance increase following the second depolarizing pulse of ΔCm_5. *E*, averaged leak-subtracted I_{Ca} measured during a 15 ms depolarization given prior to the stimulatory pulses in *B*. The bar graph displays integrated current (Q_{Ca}) normalized to cell size. $^*P < 0.05$; $^{**}P < 0.01$. Bars, means + S.E.M. Number of observations (β-cell recordings) is indicated above each averaged trace.

a limited initial size of the RRP. However, perfused islets from ashen mice exhibit a strong deficit in insulin secretion with respect to control islets in response to sustained elevated glucose exposure. Therefore, we next examined if Rab27a affects the rate at which the IRP and RRP are refilled, as may be necessary for sustained secretory responses. To examine refilling of the RRP and IRP pools, which reflects the rate of insulin granule priming, the IRP and RRP were initially depleted and then the entire ΔCm_5 and ΔCm_8 stimulation train was applied a second time following a 2 min recovery period to measure the extent to which refilling of the IRP and RRP occurred. A 2 min recovery period was chosen as it provided sufficient time for both the IRP and RRP pools to completely refill in wild-type cells (Fig. 1*B* and *D*). Comparatively, the ΔCm_5 response in *ashen* cells exhibited a ∼70% deficit in pool refilling while a ∼40% deficit was observed in the refilling of the RRP (Fig. 1*B* and *D*).

Since intracellular calcium $[Ca^{2+}]_i$ is both a stimulus for secretion and an important determinant of secretory granule priming (Gillis & Misler, 1992; Eliasson *et al.* 1996; Barg *et al.* 2001), differences in calcium dynamics between wild-type and *ashen* β-cells could potentially confound interpretation of the results. To determine if such differences occurred we quantified the total Ca^{2+} influx (integrated current, Q_{Ca}) during a 15 ms depolarizing pulse (−70 mV to +20 mV) 2 min prior to the first stimulus train under each condition. This depolarization was insufficient to evoke secretion, consistent with other reports (Barg *et al.* 2001). No difference in Q_{Ca} was found between wild-type and *ashen* β-cells (Fig. 1*E*). We also examined voltage activation relationships for the Ca^{2+} current, using 100 ms depolarizing pulses from the holding potential (−70 mV) to voltages between −70 mV and +50 mV. Peak current was elicited comparably in both wild-type and *ashen* β-cells at voltages between +20 and +30 mV (Fig. 2*A*). Also important to our investigations was demonstration that isolated *ashen* β-cells retain a glucose-induced Ca^{2+} response equivalent to that observed in β-cells from C3H/He controls. For this determination we measured the increase in $[Ca^{2+}]_i$ in *ashen* and control β-cells loaded with Fura-2 in response to 16.7 mM glucose stimulation. After a delay, which varied from 2 to 4 min, the Fura-2 340/380 intensity ratio increased 2- to 3-fold and without significant difference in both C3H/He and *ashen* β-cells in response to glucose ($n = 6$). Representative glucose-stimulated changes in Fura-2 fluorescence are displayed in Fig. 2*B*, and the averaged changes in 340/380 intensity ratio are plotted in Fig. 2*C*. Taken together, our results indicate that the deficit in vesicle pool refilling of both the IRP and RRP in *ashen* β-cells results from the absence of Rab27a and not altered Ca^{2+} dynamics or glucose responsiveness. In addition, as a reduced release of pre-docked vesicles was previously observed in *ashen* β-cells by TIRF microscopy (Kasai *et al.* 2005), our results suggest that Rab27a normally facilitates vesicle priming.

Rab27a and Rab3a act in distinct secretion amplifying pathways

In addition to Rab27a, isoforms of the small GTPase Rab3 (a/b/c/d) are present on pancreatic β-granules (Tsuboi

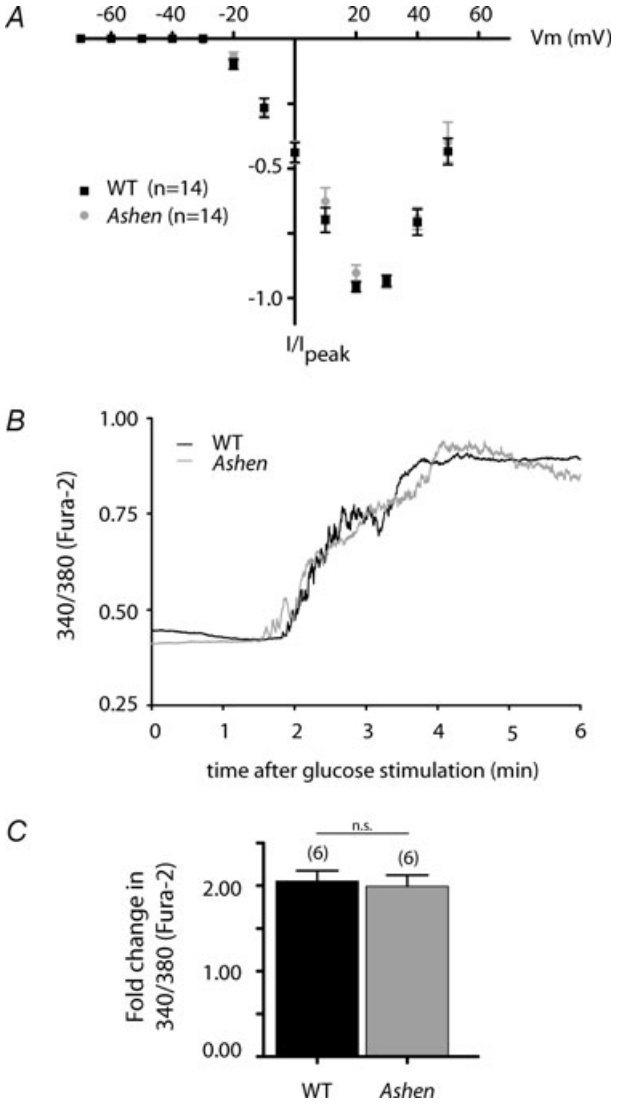

Figure 2. Comparison of ashen and wild-type β-cell voltage-gated calcium influx and of intracellular Ca^{2+} responses to glucose stimulation

A, current–voltage relationship of I_{Ca} in control C3H/He or *ashen* β-cells measured in response to 100 ms step depolarizations applied at 1 Hz from a holding potential of −70 mV. Glucose at 5 mM. *B*, representative changes in intracellular Ca^{2+} measured from single wild-type C3H/He (black) and *ashen* (grey) β-cells loaded with Fura-2 in response to 16.7 mM glucose. Prior to stimulation cells were incubated in 2.8 mM glucose for > 30 min. *C*, averaged fold-change of Fura-2 (340/380) intensity ratio measured from baseline to peak are plotted from cells in *B*. Bars, means + S.E.M. Number of observations (β-cell recordings) is indicated above each averaged trace.

& Fukuda, 2006*a*). Perfused Rab3a-null islets reportedly exhibit a decreased (by 50%) secretory response to elevated glucose (16.7 mM), when administered over 1 h (Yaekura *et al.* 2003). To compare the effects of Rab3 deficiency with that of Rab27a deficiency we measured exocytosis from pancreatic β-cells isolated from Rab3a-null mice elicited in response to the voltage depolarization protocol outlined in Fig. 1*A*. The initial size of IRP measured from Rab3a-null β-cells (13 ± 3 fF) was comparable to wild-type C57Bl/6 cells (15 ± 2 fF), and was completely refilled after a 2 min recovery period. Ca^{2+} influx between these two experiments was not significantly different (Fig. 3*C*). In response to 500 ms step depolarizations, the RRP secretory responses exhibited similar kinetics in both Rab3a$^{-/-}$ and C57Bl/6 control β-cells (Rab3a$^{-/-}$, $1/\tau = 0.30 \pm 0.06\ s^{-1}$; C57Bl/6, $1/\tau = 0.35 \pm 0.06\ s^{-1}$). However, the initial size of the RRP in Rab3a-null β-cells was substantially ($27 \pm 8\%$) smaller than C57Bl/6 cells, a deficit which was not observed in *ashen* β-cells (Fig. 1*A* and *B*). Also in contrast to *ashen* β-cells, the Rab3a-null cells demonstrated full recovery of the RRP over the 2 min period as indicated by responses to the second stimulus train (Fig. 3*A* and *B*). These results indicate that while Rab3a is more important for initial RRP size, Rab27a is a rate-limiting step in IRP and RRP refilling. This difference indicates that Rab27a and Rab3a have certain functionally distinct roles in the final signalling pathways governing insulin secretion.

Glucose-dependent vesicle priming in ashen β-cells

As established by multiple studies of single vesicle release, glucose possesses the ability to potently increase insulin secretion from pancreatic β-cells through increased priming of insulin granules into the functionally identified granule pools (Wan *et al.* 2004; Yang & Gillis, 2004). We therefore next determined the effects of a > 10 min preincubation in 16.7 mM glucose on the IRP and RRP pool size in β-cells from *ashen* and background control mice. Figure 4*A* presents the averaged capacitance responses following glucose treatment using the stimulation protocol of Fig. 1*A*. This treatment resulted in a $28 \pm 6\%$ increase in Q_{Ca} as measured by a 15 ms depolarization measured prior to the ΔCm_5 and ΔCm_8 stimulus train. Two principal differences in secretion were observed between *ashen* cells incubated in

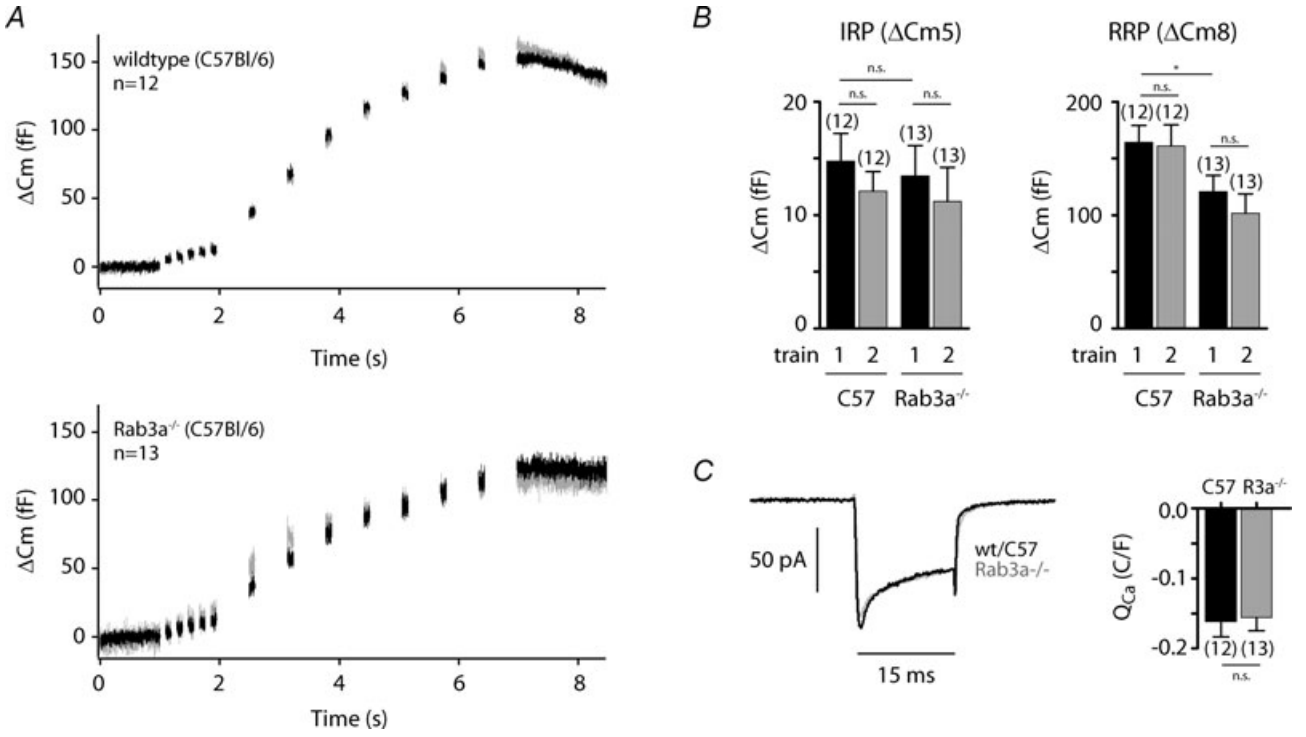

Figure 3. Measurement of IRP and RRP pool sizes and refilling in Rab3a-null β-cells
A, averaged capacitance changes measured from background control (C57) and Rab3a$^{-/-}$ β-cells in response to two depolarization trains (black, grey) as described in Fig. 1*A*. Experiments were performed in 5 mM glucose. *B*, averaged capacitance increases measured after ΔCm_5 (IRP) or ΔCm_8 (RRP) from cells in *A*. *C*, averaged leak-subtracted I_{Ca} measured during a 15 ms depolarization given prior to the stimulatory pulses in *A*. The bar graph displays integrated current (Q_{Ca}) normalized to cell size. $^*P < 0.05$; $^{**}P < 0.01$. Bars, means + S.E.M. Number of observations (β-cell recordings) is indicated above each averaged trace.

5 mM (Fig. 1) and 16.7 mM glucose (Fig. 4). First, the rate of secretion was dramatically increased by 16.7 mM glucose, as measured by an increase in the rate constant from $1/\tau = 0.63 \pm 0.09\ s^{-1}$ to $1/\tau = 1.36 \pm 0.07\ s^{-1}$ measured across the ΔCm_8. Secondly, although the magnitude of the IRP was unaffected by increasing glucose to 16.7 mM, the IRP measured after a second stimulus train completely recovered in *ashen* cells incubated in 16.7 mM glucose (Fig. 4*A* and *B*), whereas those in 5 mM glucose exhibited a ~70% deficit using the same stimulation protocol (Fig. 1*A* and *D*). However, this 'rescue' was limited to the IRP, as refilling of the RRP after 2 min remained incomplete, and was comparable in both 5 mM and 16.7 mM glucose (deficits of $42 \pm 7\%$ and $30 \pm 7\%$, respectively) (Fig. 4). Thus, our results indicate that at high concentration glucose maintains a Rab27a-independent mechanism for increasing the rate of β-granules movement from the RRP into the IRP, while the glucose-induced priming into the RRP continues to be limited by the absence of Rab27a.

cAMP-dependent vesicle priming and vesicle pool refilling in ashen β-cells

As a second messenger, cAMP stimulates exocytosis for a given Ca^{2+} influx from release-ready β-cell vesicle pools (Jones *et al.* 1986; Ammala *et al.* 1993*a*; Renstrom *et al.* 1997; Wan *et al.* 2004; Yang & Gillis, 2004). To determine the role of Rab27a in the cAMP pathway we next compared secretory responses (IRP and RRP size and rate of refilling) from *ashen* and wild-type β-cells using the stimulation protocol depicted in Fig. 1*A*. As shown in Fig. 5*A* and *B*, inclusion of 100 μM cAMP in the recording pipette solution resulted in an increase in the size of the initial IRP and RRP response that was statistically equivalent for wild-type (C3H/He) and Rab27a-null β-cells. The secretory response from C3H/He and *ashen* β-cells recorded in the absence of exogenously added cAMP are redisplayed from Fig. 1*A* for comparison. Notably, in the presence of added cAMP the ΔCm_5 elicited stepwise increases in membrane capacitance that continued throughout the series of step depolarizations, suggesting that the ΔCm_5 response may have included a contribution from the RRP. As an alternative strategy, the size of the IRP was evaluated using analysis of the first two 50 ms pulses of ΔCm_5. Figure 5*B* shows that cAMP induced a ~300% increase in the IRP size to 18 ± 3 fF in wild-type and 23 ± 4 fF in *ashen* β-cells. By comparison, the RRP increased ~40% to 185 ± 16 fF in wild-type and 190 ± 17 fF in *ashen* β-cells. In part, the increase in secretory response may be attributable to an observed effect of cAMP to slow Ca^{2+}-current inactivation in both wild-type and *ashen* β-cells (Fig. 5*C*). Of importance, *ashen* and wild-type β-cell responses evoked in response to the second stimulus train were found to be equivalent to the first secretory response when cAMP was present (Fig. 5*A* and *B*), demonstrating that the IRP and RRP are capable of complete refilling in the absence of Rab27a when cAMP signalling pathways are activated. Inclusion of cAMP in the recording pipette was also observed to result in a decrease in the rate of capacitance increase in *ashen* β-cells during the ΔCm_8 of the first stimulus train. The rate constant ($1/\tau$) of secretion without cAMP was $0.64 \pm 0.09\ s^{-1}$ while in its presence it was $0.40 \pm 0.07\ s^{-1}$. The reduction in the rate of capacitance increase in

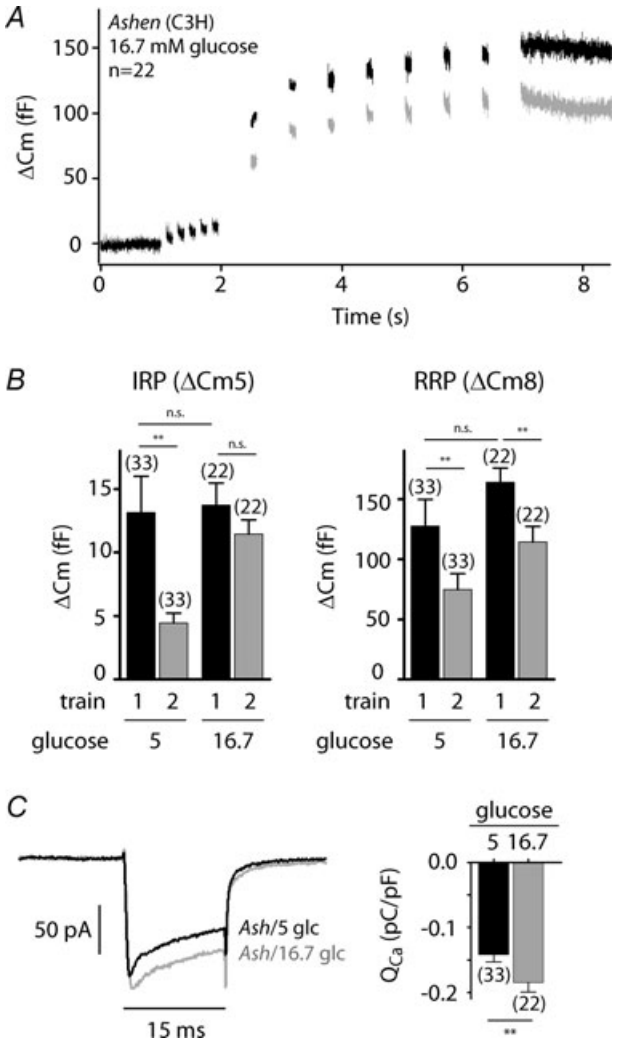

Figure 4. Glucose-dependent increases in priming of the RRP are deficient in ashen β-cells
A, averaged capacitance changes measured from *ashen* β-cells incubated in 16.7 mM glucose for > 10 min. The stimulus protocol is detailed in Fig. 1*A*. The first (black) and second (grey) stimulus trains were given 2 min apart. *B*, averaged capacitance increases measured after ΔCm_5 (IRP) or ΔCm_8 (RRP) from cells in *A*. *C*, averaged leak-subtracted I_{Ca} measured during a 15 ms depolarization given prior to the stimulatory pulses in *A*. The bar graph displays integrated current (Q_{Ca}) normalized to cell size. $^*P < 0.05$; $^{**}P < 0.01$. Bars, means + S.E.M. Number of observations (β-cell recordings) is indicated above each averaged trace.

ashen β-cells with cAMP resulted in a rate approximately equivalent to C3/He cells in the presence ($0.43 \pm 0.05\ s^{-1}$) of 100 μM cAMP. Thus, activation of cAMP signalling pathways is able to circumvent the rate-limiting effects of Rab27a on secretion.

The relative contribution of cAMP effector pathways differs in wild-type and ashen β-cells

As the addition of cAMP eliminated the secretory deficit observed in *ashen* β-cells (Fig. 5), it suggested that one or more cAMP effectors facilitates priming by acting

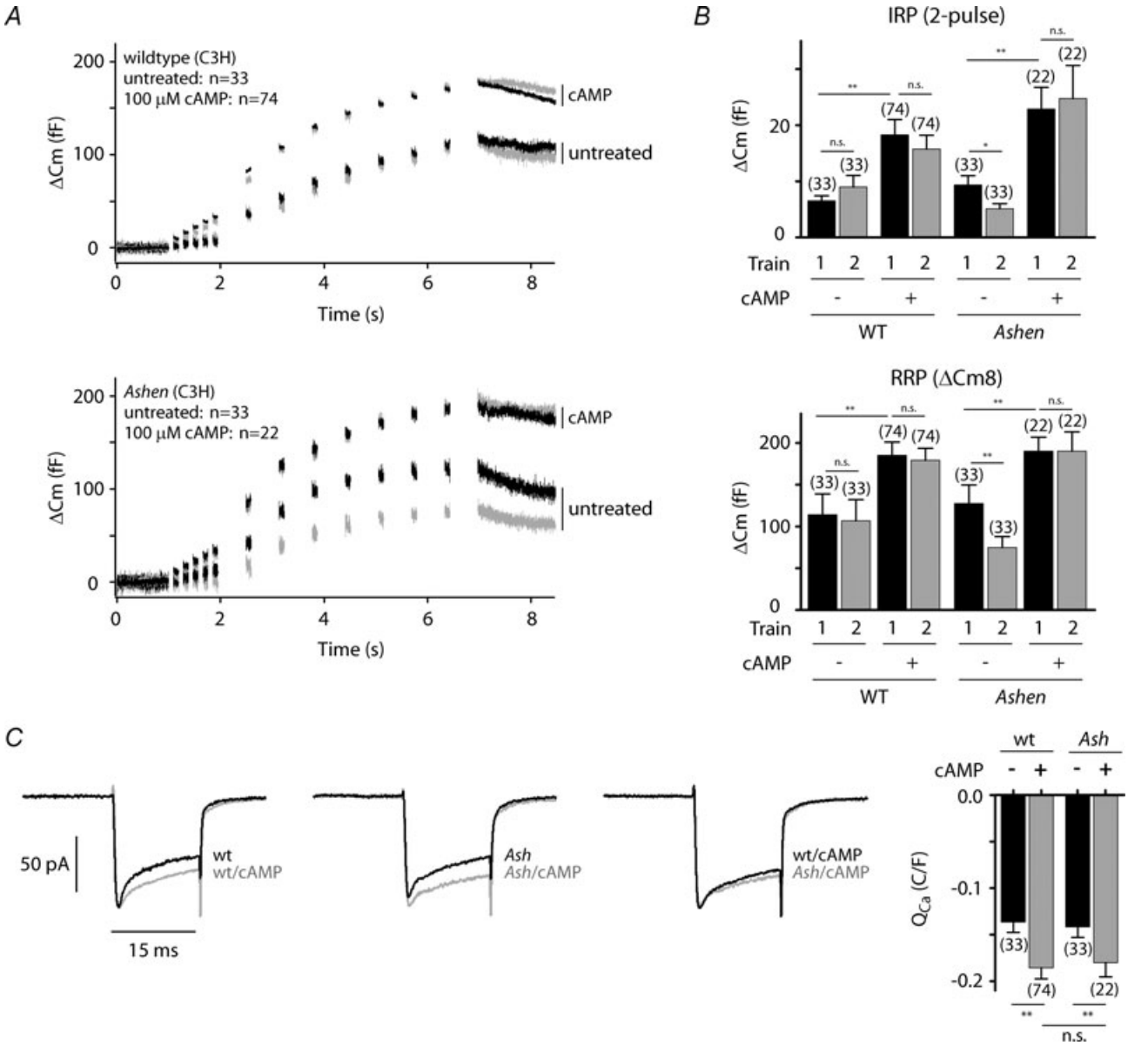

Figure 5. Effects of cAMP on evoked changes in membrane capacitance in ashen β-cells
A, averaged capacitance increases measured in response to 100 μM cAMP from wild-type (C3H/He) and *ashen* β-cells in response to two pulse trains (black, grey) described in Fig. 1*A*. Capacitance changes from untreated cells are redisplayed from Fig. 1*B* for comparison. Experiments are performed with 5 mM glucose in the bath. *B*, the IRP was analysed by the 2-pulse procedure described in Fig. 1*D*. The RRP is quantified as averaged capacitance increases measured following ΔCm_8 from cells in *A*. *C*, averaged leak-subtracted I_{Ca} measured during a 15 ms depolarization given prior to the stimulatory pulses in *A*. The bar graph displays integrated current (Q_{Ca}) normalized to cell size. $^*P < 0.05$; $^{**}P < 0.01$. Bars, means + S.E.M. Number of observations (β-cell recordings) is indicated above each averaged trace.

in exocytotic signalling pathways parallel to or downstream of Rab27a. Protein kinase A (PKA) is one such effector that directly binds cAMP and strongly modulates Ca^{2+}-triggered exocytosis in pancreatic β-cells (Gillis & Misler, 1992; Ammala *et al.* 1993*a*; Ammala *et al.* 1994; Wan *et al.* 2004; Yang & Gillis, 2004). We therefore next determined the effects of PKA on cAMP-potentiated (100 μM) insulin secretion and vesicle pool refilling in *ashen* β-cells by modifying the pipette solution to include 500 μM Rp-cAMP, which inactivates PKA (Renstrom *et al.* 1997; Wan *et al.* 2004; Yang & Gillis, 2004). As shown in Fig. 6*A* and *B*, the capacitance responses to the initial set of ΔCm_5 and ΔCm_8 stimulus depolarizations (i.e. the IRP and RRP) in the presence of cAMP and Rp-cAMP remained equivalent to that in cells treated with cAMP alone (cf. Fig. 5*A* and *B*). These results suggest that the initial enhancement of secretion by cAMP is largely facilitated by PKA-independent pathways. By comparison, the capacitance increases to application of the second pulse train after a 2 min recovery period demonstrated that while refilling of the IRP remained PKA independent, refilling of the RRP in both wild-type and *ashen* β-cells was strongly PKA dependent (Fig. 5*B*). Notably, this second pulse train elicited a 122 ± 12 fF response in C3H/He cells treated with cAMP and Rp-cAMP (Fig. 6), a response that was nearly identical to wild-type cells in the

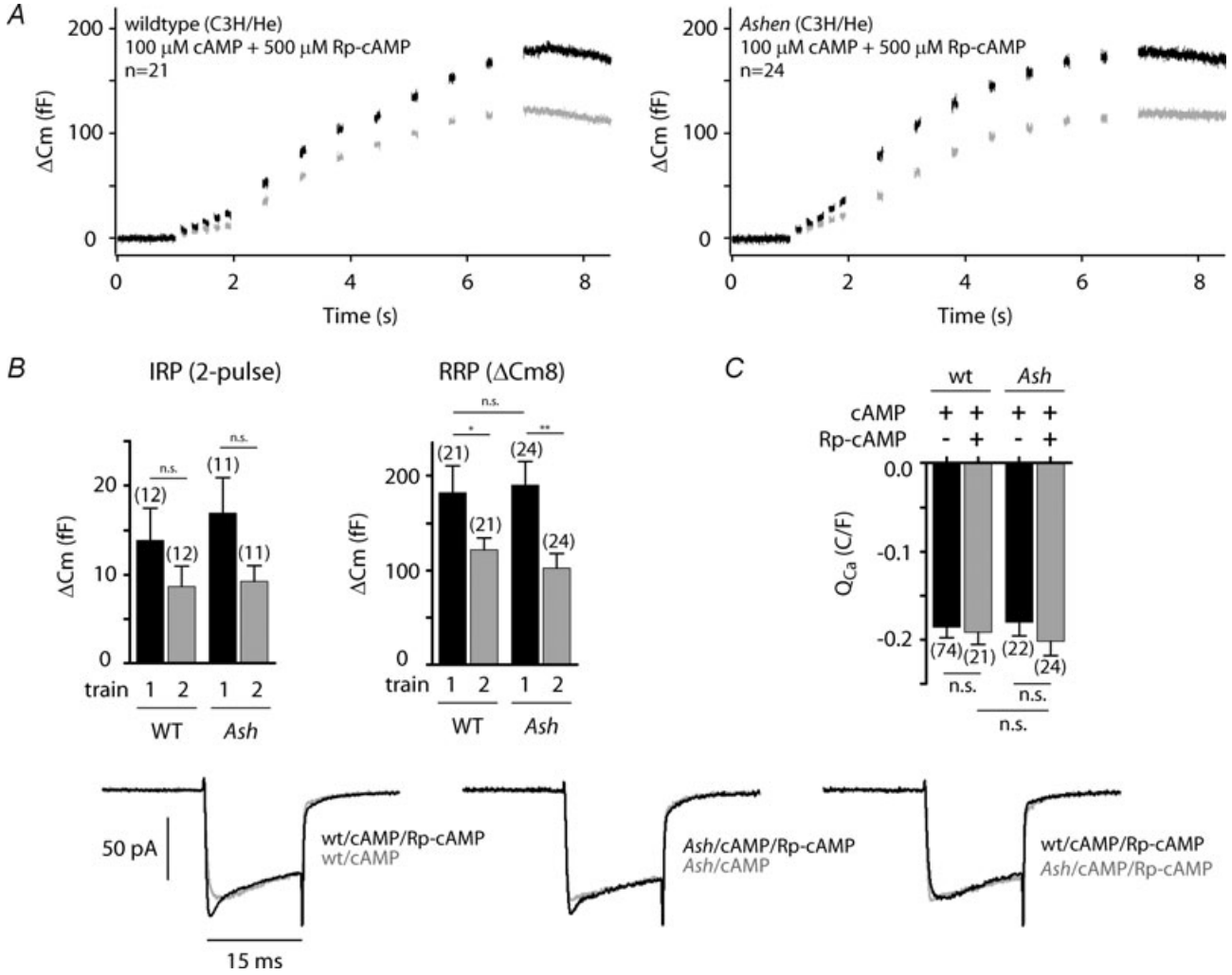

Figure 6. A PKA-dependent step downstream of Rab27a facilitates RRP pool refilling
A, averaged capacitance increases recorded from wild-type (C3H/He) and *ashen* β-cells as indicated with 100 μM cAMP and 500 μM Rp-CAMP (PKA inhibitor) in the pipette solution. Cells were stimulated by two pulse trains 2 min apart (black, grey) as described in Fig. 1*A*. *B*, averaged capacitance release from the IRP was analysed by the 2-pulse procedure as described in Fig. 1*D*. The RRP was quantified as the averaged capacitance increase following ΔCm_8 from cells in *A*. *C*, averaged leak-subtracted I_{Ca} measured during a 15 ms depolarization given prior to the stimulatory pulses in *A*. The bar graph displays integrated current (Q_{Ca}) normalized to cell size. I_{Ca} and Q_{Ca} from cells treated with cAMP are redisplayed from Fig. 4*C*. $^*P < 0.05$; $^{**}P < 0.01$. Bars, means + S.E.M. Number of observations (β-cell recordings) is indicated above each averaged trace.

absence of cAMP (Fig. 1; 114 ± 14 fF). This comparison indicates that within a 2 min time period, PKA-dependent pathways comprise almost all (> 90%) of cAMP actions to refill the RRP in C3H/He cells. Surprisingly, in *ashen* β-cells treated with cAMP/Rp-cAMP the second pulse train elicited a greater response (Fig. 6; 104 ± 12 fF) than *ashen* cells in the absence of cAMP (Fig. 1; 75 ± 14 fF), potentially indicating that cAMP-independent pathways are up-regulated in the absence of Rab27a. Collectively, these experiments argue for considerable PKA-independent actions downstream of Rab27a.

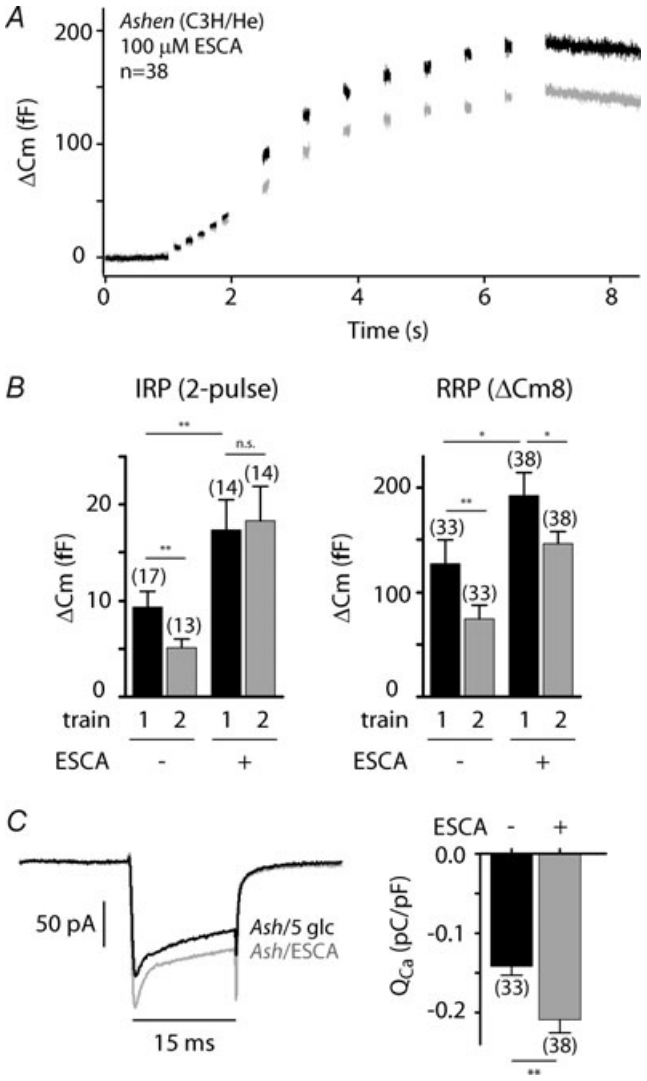

Figure 7. Effects of Epac2 activation on IRP and RRP size and refilling in ashen β-cells
A, averaged capacitance changes recorded from *ashen* β-cells in the presence of 100 μM 8-pCPT-2′-*O*-Me-cAMP (ESCA) in response to two pulse trains (black, grey) as described in Fig. 1*A*. *B*, averaged capacitance release from the IRP was analysed by the 2-pulse procedure as described in Fig. 1*D*. The RRP was quantified as the averaged capacitance increase following ΔCm_8 from cells in *A*. *C*, averaged leak-subtracted I_{Ca} measured during a 15 ms depolarization given prior to the stimulatory pulses in *A*. The bar graph displays integrated current (Q_{Ca}) normalized to cell size. $^*P < 0.05$; $^{**}P < 0.01$. Bars, means + S.E.M. Number of observations (β-cell recordings) is indicated above each averaged trace.

Contribution of Epac2 to cAMP facilitation of secretion in ashen β-cells

The experiments described above indicate that glucose-dependent deficits in pool refilling occur in *ashen* β-cells (Figs 1 and 3). In addition, we demonstrated above that cAMP-dependent pathways remain potent secretory activators in *ashen* β-cells, particularly those independent of PKA. These pathways are capable of increasing the RRP size, but are insufficient (i.e. require PKA action) to increase the rate of pool refilling following its depletion (Fig. 6). In pancreatic β-cells, PKA-independent effects of cAMP have been reported, in part, to involve activation of Epac2 (*e*xchange *p*rotein directly *a*ctivated by *c*AMP). This Epac2 pathway can be selectively activated by pharmacological ESCAs (*E*pac *s*elective *c*AMP *a*nalogues; here, 8-pCPT-2′-*O*-Me-cAMP) (Kang *et al.* 2003; Holz *et al.* 2008). Therefore, to determine the contribution of Epac2 to PKA-independent actions of cAMP in *ashen* β-cells, we measured capacitance increases to ΔCm_5 and ΔCm_8 when 100 μM ESCA was included in the pipette solution. As shown in Fig. 7, the IRP (17 ± 3 fF) and RRP size (185 ± 22 fF) measured in response to application of the initial series of depolarizing steps were similar to wild-type or *ashen* cells treated with cAMP (Fig. 5) or cAMP and Rp-cAMP (Fig. 6). This results shows that Epac2 is directly responsible for the PKA-independent boost in the IRP and RRP observed by evaluation of the first induction of pool depletion. By comparison, evaluation of refilling of the pools by application of a second stimulus series demonstrated that the IRP recovered completely while the RRP recovered to only ~80% of its initial size. Thus, the majority of PKA-independent actions in *ashen* β-cells utilize Epac2, while PKA action is responsible for most of cAMP actions on pool refilling.

Discussion

The targeting and docking of secretory granules to the plasma membrane involves the activity of Rab-GTPases. Yet, the specific functional sites that Rab proteins act in the exocytotic pathway to mediate their actions, as well as the molecular complexes that assemble and disassemble to perform their functions, remain ill defined. In this study we have used a functional analysis of secretion to identify specific steps in the final stages of insulin secretion where Rab27a acts. The experiments compared secretory responses from *ashen* β-cells (which lack Rab27a

protein) and Rab3a$^{-/-}$ β-cells with appropriate background control β-cells. Multiple sites of Rab27a action were identified including regulation of the rate of refilling of specific readily releasable granule pools. In addition, we identify a role for Rab27a that limits the rate of granule fusion from these pools with the plasma membrane. Moreover, we find that these functions are unique to Rab27a, as Rab3a, which is also present on insulin secretory granules, did not exert regulation at these steps. Both the deficit in pool refilling in the *ashen* β-cells and the increased rate of pool depletion were not observed in the presence of cAMP, owing largely to PKA-dependent pathways. Collectively, our results suggest that glucose-dependent enhancement of insulin secretion involves priming pathways that utilize Rab27a while, by comparison, receptor-mediated cAMP-dependent pathways that amplify secretory responses work primarily downstream of, or in parallel to, Rab27a.

What are the sites of Rab27a action in the pancreatic β-cell secretory pathway?

We have used stimulus-induced changes in membrane capacitance as a time resolved measurement of insulin release from the readily releasable pool (RRP) of insulin granules (~60 granules), and its kinetically distinct subset of ~10 Ca^{2+} channel-associated immediately releasable granules (IRP) (Barg *et al.* 2001; Wan *et al.* 2004; Yang & Gillis, 2004). The functional significance of this *in situ* measurement is that *in vivo*, IRP and RRP release are believed to account for first-phase insulin secretion (via K_{ATP} channel-dependent pathways), while the sustained second-phase release requires their refilling from a reserve pool (involving K_{ATP} channel-independent pathways) (Eliasson *et al.* 1996; Barg *et al.* 2001, 2002; Olofsson *et al.* 2002; Straub & Sharp, 2002). Notably, the rate of secretion using membrane depolarization to induce Ca^{2+} influx is artificially high (~75 granules s^{-1}) (Kanno *et al.* 2004), at least ~300-fold faster than glucose-stimulated first-phase release (~0.25 granules s^{-1}) (Bratanova-Tochkova *et al.* 2002; Straub & Sharp, 2002), thereby allowing us to completely deplete both the IRP and RRP, and examine refilling processes in a shortened time frame. Using this approach, we were able to define multiple rate-limiting sites of Rab27a action in the vesicle secretory pathway.

We report that following depletion, the refilling of the RRP and IRP was incomplete even after a 2 min recovery in Rab27a-null *ashen* β-cells, compared with complete recovery seen in background control (C3H/He) cells. This result is highly significant, as a previous study suggests that the RRP recovers with a time constant of 31 s, and only 60 s is required for complete recovery (Gromada *et al.* 1999). The currently available literature on Rab27a, which has been largely derived from *ashen* mice, suggests three possible sites of Rab27a action in the secretory pathway which could potentially explain this phenomenon: granule recruitment, docking and priming. The role of Rab27a in recruitment is evidenced by the failure of melanosomes to target to the plasma membrane, accumulating around the nucleus in *ashen* melanocytes because a Rab27a-MyRIP-myosin Va tripartite complex is required for their transfer from microtubules to actin filaments (Fukuda *et al.* 2002; Strom *et al.* 2002; Waselle *et al.* 2003). Rab27a is also known to participate in granule docking. In cytotoxic T-cells (CTLs) derived from *ashen* mice, EM analysis has revealed that lytic granules polarize correctly to the immunological synapse (i.e. recruitment processes are functional), but the CTLs are unable to secrete granzyme A or hexoaminidase because the lytic granules stop short of docking (Stinchcombe *et al.* 2001). However, recruitment/docking seems unlikely to completely account for the Rab27a-dependent secretory deficit we find in *ashen* β-cells, since EM analysis has shown that the granule density at/near the PM (within 500 nm) is nearly identical in unstimulated Rab27a-null and C3H/He β-cells (Kasai *et al.* 2005), and is not affected by RNAi directed against Rab27a (Waselle *et al.* 2003). We additionally demonstrated that, functionally, the initial secretory responses between *ashen* and control β-cells were similar, yielding a ~10 fF IRP (~6 granules) and a ~115 fF RRP (~68 granules), which is comparable to control responses reported in prior studies.

We propose that Rab27a participates in glucose-dependent *priming* pathways in pancreatic β-cells. The hypothesis that Rab27a participates in priming was suggested by a dramatically reduced release of pre-docked granules seen in the total internal reflection fluorescence microscopy (TIRFM) field following glucose stimulation in *ashen* β-cells (Kasai *et al.* 2005). That priming of granules occurs in β-cells was originally suggested by quantitative comparisons between EM ultrastructural analysis and membrane capacitance measurements. Out of the ~10 000–13 000 granules in the β-cell, ~600 (~5% in total) are docked at the plasma membrane and yet only ~60 granules (~0.5% in total) comprise the RRP (Dean, 1973; Renstrom *et al.* 1997; Olofsson *et al.* 2002; Bratanova-Tochkova *et al.* 2002). Although a number of readily releasable granules have been found by TIRFM to be released without an extended docking step (described as restless newcomer granules) during first phase-secretion under glucose stimulation (Shibasaki *et al.* 2007), this population is far less affected by the absence of Rab27a than the docked pool (Kasai *et al.* 2005). We have found additionally that movement from the RRP into the IRP is strongly dependent on Rab27a at 5 mM glucose, but independent of Rab27a when extracellular glucose is raised to 16.7 mM.

By fitting the time course of RRP depletion to a single exponential, and comparing the results between *ashen* and control β-cells, we have also discovered

that Rab27a exerts a previously unknown rate-limiting action on vesicle release. The results establish a ∼2-fold faster pool depletion in *ashen* β-cells than in wild-type β-cells incubated in 5 mM glucose (*ashen*, $1/\tau = 0.63 \pm 0.09\ s^{-1}$; C3H/He, $1/\tau = 0.32 \pm 0.06\ s^{-1}$), which is further enhanced in 16.7 mM glucose (*ashen*, $1/\tau = 1.36 \pm 0.07\ s^{-1}$). A role for Rab27a action immediately proximal to secretion is evidenced by a corresponding hydrolysis of Rab-GTP upon stimulation (Kondo *et al.* 2006). This regulatory effect of Rab27a on rate of pool depletion is not recapitulated by deletion of Rab3a (Rab3a$^{-/-}$, $1/\tau = 0.30 \pm 0.06\ s^{-1}$; C57Bl/6, $1/\tau = 0.35 \pm 0.06\ s^{-1}$). Rab27a control over vesicle pool depletion is, however, bypassed by the actions of cAMP (*ashen*/cAMP, $1/\tau = 0.40 \pm 0.07\ s^{-1}$; C3H/He/cAMP, $1/\tau = 0.43 \pm 0.05\ s^{-1}$). These results support a convergence of cAMP and glucose-dependent priming pathways proximal to secretion.

The role of Rab27a effectors in glucose and Rab27a-dependent priming

Both the glucose-dependent deficit in granule pool refilling and the increased rate of RRP depletion we find in *ashen* β-cells are consistent with the known properties of Rab27a effector interactions in priming. For example, reduction of the Rab 3/27a effector Noc2 by RNAi decreases insulin secretion from INS-1 β-cells. *In vitro*, Noc2 has been reported to bind the essential priming factor Munc13 (Cheviet *et al.* 2004). Another principal Rab27a effector is Slp4a/granuphilin (Fukuda, 2005). Rab27a-dependent defects in RRP refilling could also be explained, in part, by the finding that β-cells deficient in either Rab27a (Kasai *et al.* 2005) or Slp4a (Gomi *et al.* 2005) have reductions in the number of insulin granules docked to the plasma membrane, resulting in mass action effects on priming. Although the docking of β-granules to the plasma membrane is strongly facilitated by Rab27a and Slp4a, these vesicles may be forced into an inactive and unprimed state since secretion is strongly inhibited by Slp4a overexpression (Coppola *et al.* 2002; Torii *et al.* 2002), and because Slp4a interacts strongly with only the closed and SNARE-pairing inactive Munc18/syntaxin complex (Coppola *et al.* 2002; Torii *et al.* 2002; Gomi *et al.* 2005; Tsuboi & Fukuda, 2006*b*). This biochemical state could explain the Rab27a-dependent clamp on granule release absent in *ashen* β-cells. Indeed, the clamp may be released upon stimulation, as Rab27a undergoes GTP hydrolysis, which is known to accompany stimulation (Kondo *et al.* 2006).

The interplay of Rab27a and Rab3a in priming pathways

Islets isolated from either Rab27a-null (Kasai *et al.* 2005) or Rab3a-null (Yaekura *et al.* 2003) animals are reported to exhibit glucose intolerance as well as a ∼50% defect in glucose-stimulated insulin secretion. Our results identify the site of the Rab27a-dependent secretion deficit as a glucose-dependent defect in IRP and RRP refilling, yet as we see no initial deficit in the RRP size, it is surprising that Rab27a-null animals are glucose intolerant (Kasai *et al.* 2005). Notably, the functionally defined Rab27a deficits in secretion were not observed in Rab3a-null β-cells, suggesting that the two molecules do not function redundantly in pancreatic β-cells. This is an important determination when one considers that some redundancy exists in Rab27 and Rab3 effector interactions. For example, rabphilin and Noc2, which were first characterized as Rab3a effectors (Kotake *et al.* 1997; Haynes *et al.* 2001), also function in concert with Rab27a (Cheviet *et al.* 2004; Fukuda *et al.* 2004). Slp4a, however, is believed to form an endogenous complex only with Rab27a based on its high affinity interaction (Mahoney *et al.* 2006), despite its interaction with Rab3a *in vitro* (Coppola *et al.* 2002). Moreover, the Munc13–1 binding protein RIM (Betz *et al.* 2001) only binds to Rab3a (Fukuda, 2005). The situation in other cell types may be different. For example, in PC12 cells, RNAi knockdown of Rab27a and Rab3a has an additive effect to reduce secretion (Tsuboi & Fukuda, 2006*a*). It seems more likely, though, that Rab3a is redundant with the other three isoforms present on β-granules (i.e. Rab a/b/c/d) (Iezzi *et al.* 1999).

Rab27a and amplifying pathways of secretion

The effects of cAMP to augment secretion are furthermore additive with those seen under conditions of elevated glucose (Wan *et al.* 2004; Yang & Gillis, 2004), suggesting that at least some glucose and cAMP signalling intermediates act in independent pathways. We have found that the actions of cAMP have two principal effects independent of the glucose/Rab27a-dependent pathways on pool size and refilling. First, cAMP can quickly enhance (in < 3 min) the initial IRP and RRP magnitude in *ashen* β-cells to an equivalent extent as in control β-cells. Second, cAMP can obviate the Rab27a-dependent deficit in pool refilling seen in the *ashen* cells. The intracellular mediators of these cAMP effects are separable into PKA-independent and PKA-dependent pathways, respectively.

Our results indicate that cAMP-mediated refilling of the RRP is strongly dependent on PKA, since Rp-cAMP completely blocks the ability of cAMP to refill the RRP in both wild-type and *ashen* β-cells. Consequently, we find no Rab27a dependence of PKA action. Interestingly, we found that Rp-cAMP has no effect in limiting the initial enhancement of the IRP and RRP by cAMP. This is surprising, since previous reports using the same inhibitor describe a partial (Rosengren *et al.* 2002) or complete block (Wan *et al.* 2004; Yang & Gillis, 2004) of an initial

cAMP-induced enhancement of depolarization-induced exocytosis. Perhaps the inhibition by Rp-cAMP lags behind cAMP activation, in spite of the high Rp-cAMP concentration we used in the patch pipette. On the other hand, it may be that the activity of PKA is only evident after stimulation, during the refilling of the IRP and RRP (i.e. the observed initial boost in RRP size prior to its depletion is likely to be mediated by PKA-independent pathways). Renstrom *et al.* (1997) previously reported that neither Rp-cAMP nor PKI (PKA inhibitory peptide) affected cAMP potentiation of granule release evoked by a single 500 ms depolarizing pulse, but when additional pulses are applied at 1 Hz over tens of seconds, where RRP refilling processes would predominate, the effects of cAMP to enhance secretion are severely reduced by PKA inhibition. Consistent with this latter hypothesis, we found that direct activation of Epac2 in *ashen* cells with the ESCA 8-pCPT-2′-O-Me-cAMP increased the initial RRP size (closely mimicking the treatment of *ashen* cells with cAMP/Rp-cAMP), but failed to support complete refilling of the RRP.

Summary

Interactions between Rab27a-GTPase and its effectors on secretory granule membrane are believed to act in concert with SNAREs on the plasma membrane to facilitate docking and secretion. In this study we have investigated the mechanisms by which insulin secretion is regulated by Rab27a in mouse pancreatic β-cells, focusing specifically on the glucose- and cAMP-dependent priming pathways. Our results indicate that Rab27a is a central effector upon which glucose-dependent β-cell signalling pathways converge to regulate refilling of and rate of release from specific releasable pools of secretory granules. Moreover, Rab27a and Rab3a appear not to be redundant in their actions. Finally, cAMP amplification of insulin secretion acts primarily downstream of or independent of Rab27a, suggesting Rab27a is a critical regulator of glucose-induced secretion and an important mediator of both first and second phase of glucose stimulated insulin secretion.

References

Ammala C, Ashcroft FM & Rorsman P (1993*a*). Calcium-independent potentiation of insulin release by cyclic AMP in single β-cells. *Nature* **363,** 356–358.

Ammala C, Eliasson L, Bokvist K, Berggren PO, Honkanen RE, Sjoholm A & Rorsman P (1994). Activation of protein kinases and inhibition of protein phosphatases play a central role in the regulation of exocytosis in mouse pancreatic β-cells. *Proc Natl Acad Sci U S A* **91,** 4343–4347.

Ammala C, Eliasson L, Bokvist K, Larsson O, Ashcroft FM & Rorsman P (1993*b*). Exocytosis elicited by action potentials and voltage-clamp calcium currents in individual mouse pancreatic β-cells. *J Physiol* **472,** 665–688.

Barg S, Eliasson L, Renstrom E & Rorsman P (2002). A subset of 50 secretory granules in close contact with L-type Ca^{2+} channels accounts for first-phase insulin secretion in mouse β-cells. *Diabetes* **51** (Suppl. 1), S74–S82.

Barg S, Ma X, Eliasson L, Galvanovskis J, Gopel SO, Obermuller S, Platzer J, Renstrom E, Trus M, Atlas D, Striessnig J & Rorsman P (2001). Fast exocytosis with few Ca^{2+} channels in insulin-secreting mouse pancreatic β-cells. *Biophys J* **81,** 3308–3323.

Betz A, Thakur P, Junge HJ, Ashery U, Rhee JS, Scheuss V, Rosenmund C, Rettig J & Brose N (2001). Functional interaction of the active zone proteins Munc13–1 and RIM1 in synaptic vesicle priming. *Neuron* **30,** 183–196.

Bratanova-Tochkova TK, Cheng H, Daniel S, Gunawardana S, Liu YJ, Mulvaney-Musa J, Schermerhorn T, Straub SG, Yajima H & Sharp GW (2002). Triggering and augmentation mechanisms, granule pools, and biphasic insulin secretion. *Diabetes* **51** (Suppl. 1), S83–S90.

Burgoyne RD & Morgan A (2003). Secretory granule exocytosis. *Physiol Rev* **83,** 581–632.

Cheviet S, Coppola T, Haynes LP, Burgoyne RD & Regazzi R (2004). The Rab-binding protein Noc2 is associated with insulin-containing secretory granules and is essential for pancreatic b-cell exocytosis. *Mol Endocrinol* **18,** 117–126.

Coppola T, Frantz C, Perret-Menoud V, Gattesco S, Hirling H & Regazzi R (2002). Pancreatic b-cell protein granuphilin binds Rab3 and Munc-18 and controls exocytosis. *Mol Biol Cell* **13,** 1906–1915.

Dean PM (1973). Ultrastructural morphometry of the pancreatic b-cell. *Diabetologia* **9,** 115–119.

de Wit H, Cornelisse LN, Toonen RF & Verhage M (2006). Docking of secretory vesicles is syntaxin dependent. *PLoS ONE* **1,** e126.

Eliasson L, Renstrom E, Ammala C, Berggren PO, Bertorello AM, Bokvist K, Chibalin A, Deeney JT, Flatt PR, Gabel J, Gromada J, Larsson O, Lindstrom P, Rhodes CJ & Rorsman P (1996). PKC-dependent stimulation of exocytosis by sulfonylureas in pancreatic β cells. *Science* **271,** 813–815.

Eliasson L, Renstrom E, Ding WG, Proks P & Rorsman P (1997). Rapid ATP-dependent priming of secretory granules precedes Ca^{2+}-induced exocytosis in mouse pancreatic β-cells. *J Physiol* **503,** 399–412.

Fukuda M (2003). Slp4-a/granuphilin-a inhibits dense-core vesicle exocytosis through interaction with the GDP-bound form of Rab27A in PC12 cells. *J Biol Chem* **278,** 15390–15396.

Fukuda M (2005). Versatile role of Rab27 in membrane trafficking: focus on the Rab27 effector families. *J Biochem (Tokyo)* **137,** 9–16.

Fukuda M, Kanno E & Yamamoto A (2004). Rabphilin and Noc2 are recruited to dense-core vesicles through specific interaction with Rab27A in PC12 cells. *J Biol Chem* **279,** 13065–13075.

Fukuda M, Kuroda TS & Mikoshiba K (2002). Slac2-a/melanophilin, the missing link between Rab27 and myosin Va: implications of a tripartite protein complex for melanosome transport. *J Biol Chem* **277,** 12432–12436.

Gillis KD & Misler S (1992). Single cell assay of exocytosis from pancreatic islet β cells. *Pflugers Arch* **420,** 121–123.

Gillis KD, Mossner R & Neher E (1996). Protein kinase C enhances exocytosis from chromaffin cells by increasing the size of the readily releasable pool of secretory granules. *Neuron* **16,** 1209–1220.

Gomi H, Mizutani S, Kasai K, Itohara S & Izumi T (2005). Granuphilin molecularly docks insulin granules to the fusion machinery. *J Cell Biol* **171,** 99–109.

Gromada J, Hoy M, Renstrom E, Bokvist K, Eliasson L, Gopel S & Rorsman P (1999). CaM kinase II-dependent mobilization of secretory granules underlies acetylcholine-induced stimulation of exocytosis in mouse pancreatic β-cells. *J Physiol* **518,** 745–759.

Gulyas-Kovacs A, de Wit H, Milosevic I, Kochubey O, Toonen R, Klingauf J, Verhage M & Sorensen JB (2007). Munc18–1: sequential interactions with the fusion machinery stimulate vesicle docking and priming. *J Neurosci* **27,** 8676–8686.

Haynes LP, Evans GJ, Morgan A & Burgoyne RD (2001). A direct inhibitory role for the Rab3-specific effector, Noc2, in Ca^{2+}-regulated exocytosis in neuroendocrine cells. *J Biol Chem* **276,** 9726–9732.

Holz GG, Chepurny OG & Schwede F (2008). Epac-selective cAMP analogs: new tools with which to evaluate the signal transduction properties of cAMP-regulated guanine nucleotide exchange factors. *Cell Signal* **20,** 10–20.

Hume AN, Collinson LM, Rapak A, Gomes AQ, Hopkins CR & Seabra MC (2001). Rab27a regulates the peripheral distribution of melanosomes in melanocytes. *J Cell Biol* **152,** 795–808.

Iezzi M, Escher G, Meda P, Charollais A, Baldini G, Darchen F, Wollheim CB & Regazzi R (1999). Subcellular distribution and function of Rab3A, B, C, and D isoforms in insulin-secreting cells. *Mol Endocrinol* **13,** 202–212.

Jones PM, Fyles JM & Howell SL (1986). Regulation of insulin secretion by cAMP in rat islets of Langerhans permeabilised by high-voltage discharge. *FEBS Lett* **205,** 205–209.

Kang L, He Z, Xu P, Fan J, Betz A, Brose N & Xu T (2006). Munc13–1 is required for the sustained release of insulin from pancreatic β cells. *Cell Metab* **3,** 463–468.

Kang G, Joseph JW, Chepurny OG, Monaco M, Wheeler MB, Bos JL, Schwede F, Genieser HG & Holz GG (2003). Epac-selective cAMP analog 8-pCPT-2ċ-O-Me-cAMP as a stimulus for Ca^{2+}-induced Ca^{2+} release and exocytosis in pancreatic β-cells. *J Biol Chem* **278,** 8279–8285.

Kanno T, Ma X, Barg S, Eliasson L, Galvanovskis J, Gopel S, Larsson M, Renstrom E & Rorsman P (2004). Large dense-core vesicle exocytosis in pancreatic β-cells monitored by capacitance measurements. *Methods* **33,** 302–311.

Kasai K, Ohara-Imaizumi M, Takahashi N, Mizutani S, Zhao S, Kikuta T, Kasai H, Nagamatsu S, Gomi H & Izumi T (2005). Rab27a mediates the tight docking of insulin granules onto the plasma membrane during glucose stimulation. *J Clin Invest* **115,** 388–396.

Kinard TA & Satin LS (1995). An ATP-sensitive Cl^- channel current that is activated by cell swelling, cAMP, and glyburide in insulin-secreting cells. *Diabetes* **44,** 1461–1466.

Kondo H, Shirakawa R, Higashi T, Kawato M, Fukuda M, Kita T & Horiuchi H (2006). Constitutive GDP/GTP exchange and secretion-dependent GTP hydrolysis activity for Rab27 in platelets. *J Biol Chem* **281,** 28657–28665.

Kotake K, Ozaki N, Mizuta M, Sekiya S, Inagaki N & Seino S (1997). Noc2, a putative zinc finger protein involved in exocytosis in endocrine cells. *J Biol Chem* **272,** 29407–29410.

Mahoney TR, Liu Q, Itoh T, Luo S, Hadwiger G, Vincent R, Wang ZW, Fukuda M & Nonet ML (2006). Regulation of synaptic transmission by RAB-3 and RAB-27 in *Caenorhabditis elegans*. *Mol Biol Cell* **17,** 2617–2625.

Miley HE, Brown PD & Best L (1999). Regulation of a volume-sensitive anion channel in rat pancreatic β-cells by intracellular adenine nucleotides. *J Physiol* **515,** 413–417.

Olofsson CS, Gopel SO, Barg S, Galvanovskis J, Ma X, Salehi A, Rorsman P & Eliasson L (2002). Fast insulin secretion reflects exocytosis of docked granules in mouse pancreatic β-cells. *Pflugers Arch* **444,** 43–51.

Renstrom E, Eliasson L & Rorsman P (1997). Protein kinase A-dependent and-independent stimulation of exocytosis by cAMP in mouse pancreatic β-cells. *J Physiol* **502,** 105–118.

Rosengren A, Filipsson K, Jing XJ, Reimer MK & Renstrom E (2002). Glucose dependence of insulinotropic actions of pituitary adenylate cyclase-activating polypeptide in insulin-secreting INS-1 cells. *Pflugers Arch* **444,** 556–567.

Shibasaki T, Takahashi H, Miki T, Sunaga Y, Matsumura K, Yamanaka M, Zhang C, Tamamoto A, Satoh T, Miyazaki J & Seino S (2007). Essential role of Epac2/Rap1 signaling in regulation of insulin granule dynamics by cAMP. *Proc Natl Acad Sci U S A* **104,** 19333–19338.

Stinchcombe JC, Barral DC, Mules EH, Booth S, Hume AN, Machesky LM, Seabra MC & Griffiths GM (2001). Rab27a is required for regulated secretion in cytotoxic T lymphocytes. *J Cell Biol* **152,** 825–834.

Straub SG & Sharp GW (2002). Glucose-stimulated signaling pathways in biphasic insulin secretion. *Diabetes Metab Res Rev* **18,** 451–463.

Strom M, Hume AN, Tarafder AK, Barkagianni E & Seabra MC (2002). A family of Rab27-binding proteins. Melanophilin links Rab27a and myosin Va function in melanosome transport. *J Biol Chem* **277,** 25423–25430.

Takahashi N, Kadowaki T, Yazaki Y, Miyashita Y & Kasai H (1997). Multiple exocytotic pathways in pancreatic β cells. *J Cell Biol* **138,** 55–64.

Torii S, Zhao S, Yi Z, Takeuchi T & Izumi T (2002). Granuphilin modulates the exocytosis of secretory granules through interaction with syntaxin 1a. *Mol Cell Biol* **22,** 5518–5526.

Tsuboi T & Fukuda M (2006*a*). Rab3A and Rab27A cooperatively regulate the docking step of dense-core vesicle exocytosis in PC12 cells. *J Cell Sci* **119,** 2196–2203.

Tsuboi T & Fukuda M (2006*b*). The Slp4-a linker domain controls exocytosis through interaction with Munc18–1.syntaxin-1a complex. *Mol Biol Cell* **17,** 2101–2112.

Voets T, Toonen RF, Brian EC, de Wit H, Moser T, Rettig J, Sudhof TC, Neher E & Verhage M (2001). Munc18–1 promotes large dense-core vesicle docking. *Neuron* **31,** 581–591.

Wan QF, Dong Y, Yang H, Lou X, Ding J & Xu T (2004). Protein kinase activation increases insulin secretion by sensitizing the secretory machinery to Ca^{2+}. *J Gen Physiol* **124,** 653–662.

Wang X, Thiagarajan R, Wang Q, Tewolde T, Rich MM & Engisch KL (2008). Regulation of quantal shape by Rab3A: evidence for a fusion pore-dependent mechanism. *J Physiol* **586,** 3949–3962.

Waselle L, Coppola T, Fukuda M, Iezzi M, El-Amraoui A, Petit C & Regazzi R (2003). Involvement of the Rab27 binding protein Slac2c/MyRIP in insulin exocytosis. *Mol Biol Cell* **14,** 4103–4113.

Wilson SM, Yip R, Swing DA, O'Sullivan TN, Zhang Y, Novak EK, Swank RT, Russell LB, Copeland NG & Jenkins NA (2000). A mutation in Rab27a causes the vesicle transport defects observed in ashen mice. *Proc Natl Acad Sci U S A* **97,** 7933–7938.

Wu X, Wang F, Rao K, Sellers JR & Hammer JA 3rd (2002). Rab27a is an essential component of melanosome receptor for myosin Va. *Mol Biol Cell* **13,** 1735–1749.

Yaekura K, Julyan R, Wicksteed BL, Hays LB, Alarcon C, Sommers S, Poitout V, Baskin DG, Wang Y, Philipson LH & Rhodes CJ (2003). Insulin secretory deficiency and glucose intolerance in Rab3A null mice. *J Biol Chem* **278,** 9715–9721.

Yang Y & Gillis KD (2004). A highly Ca^{2+}-sensitive pool of granules is regulated by glucose and protein kinases in insulin-secreting INS-1 cells. *J Gen Physiol* **124,** 641–651.

Yi Z, Yokota H, Torii S, Aoki T, Hosaka M, Zhao S, Takata K, Takeuchi T & Izumi T (2002). The Rab27a/granuphilin complex regulates the exocytosis of insulin-containing dense-core granules. *Mol Cell Biol* **22,** 1858–1867.

Acknowledgements

We would like to thank Dr Nancy Jenkins for providing the *ashen* mice and Dr Kathrin Engisch for providing the $Rab3a^{-/-}$ mice. This work was supported by grants from the NIH (NS053978), NIDDK (DK077050), and NIDDK DK020572 administered by the Michigan Diabetes Research and Training Center (MDRTC).